Evaluating the influence of residual stresses and surface damage on fatigue life of Nickel superalloys

R.M.N. Fleury[a,*], D. Nowell[a]

[a]*Department of Engineering Science, University of Oxford, Parks Road, OX1 3PJ, Oxford, UK*

Abstract

The effect of surface damage, such as dents caused due to the low velocity impact of hard blunt objects, on the fatigue life of mechanical components are investigated in this paper. A two-dimensional dislocation density approach is used to obtain the stress intensity factors of a crack propagating under dents. Both the contributions of the geometrical stress concentrator (notch), due to the presence of the dent, and the residual stress field, generated during the impact, on the stress intensity factor of the crack are obtained. A short crack growth model is then used to predict the fatigue life of nickel superalloys in the presence of two dent depths. The effect of the residual stress field has been shown to be the main contributor to the difference observed in predicted fatigue life between the two dent depths analysed.

Keywords: surface damage; residual stresses; fatigue; crack propagation; Nickel superalloys

1. Introduction

The effect of handling and service surface damage on the fatigue life of components of gas-turbines has increasingly been the focus of research by aero-engine manufacturers. Surface anomalies on engine parts may occur during manufacturing and maintenance due to low velocity impacts by hard objects, e.g. tool dropping or one part striking another during transport. Typically, these impacts cause dents and scratches on the surface of gas-turbine components. Current evaluation methods of the effect of dents and scratches on aero-engine components service lives follow a very conservative approach of assuming the damage as a propagating crack. This approach takes into account neither the residual stress field generated near the damage nor the time that it takes for the crack to initiate at the stress concentrator. This conservative approach implies a lower accuracy in predicting the fatigue life of components and higher cost associated with maintenance of aero-engines throughout their service life.

Mall et al. [1], when investigating the effect of foreign object damage (FOD) on Ti alloys, found that three main issues affect the fatigue life of components in the presence of surface dents: (i) the geometrical stress concentration under the 'notch' (i.e. dent); (ii) the residual stress field

*Corresponding author.
Email address: rodolfo.fleury@eng.ox.ac.uk (R.M.N. Fleury)

created during the impact; and (iii) the micro-structural changes due to the deformation. Although FOD occur due to much higher impact velocity events, most aspects of FOD are also true for handling surface damage. Using a potential drop technique, experiments undertaken by Groudin et al. [2] have shown that compressive residual stresses due to the impact of objects significantly slow down crack growth in dented and scratched specimens. A similar study was carried out by Doremus et al. [3] using Inconel 718 specimens. They have shown that the initiation life in dented specimens, which had sharp internal corners, reduces once the residual stresses are removed, whereas scratches show the opposite effect.

Finite element models have been used to simulate various impact problems and the residual stresses caused by them. Boyce et al. [4] investigated the residual stress due to the impact of a spherical projectile on Ti alloys. They suggested that impact events of low impact velocities ($<$ 200 m/s) can be modelled using a quasi-static approach. Doremus et al. [3] also used a quasi-static model to simulate scratch and sharp dent damage. Higher velocity events such as FOD have been modelled by explicit finite element code [5]. Duó et al. [6] have used laboratory and synchrotron X-ray diffraction (XRD) to measure the residual stresses caused by FOD and validate the explicit finite element code. Comparison between FE models and XRD residual stress measurements can also be found in [7, 8]. More recently, a model was developed to predict low impact velocity blunt damage in Nickel superalloys [9]. The model was validated by comparing the geometry of the dent and the residual stress under the dent by laboratory XRD.

Several authors have investigated the impact of FOD on low and high cycle fatigue crack growth [10–12]. Particularly, Nowell et al. [13] and Oakley and Nowell [14] investigated the impact of FOD on fatigue life of turbine blades using a dislocation density method [15, 16]. In this paper, we use the FE model validated in [9] to obtain the geometry and residual stress field around blunt dents of different depths. Then, a dislocation density approach is used to obtain the stress intensity factors of a crack propagating under the dents, and in the presence of the residual stress field. Fatigue life predictions are carried out by using the calculated stress intensity factors together with short and long crack propagation laws.

2. Numerical simulation of damage

2.1. Finite element model

The dents and their respective residual stress field generated due to the impact of a hardened steel blunt indenter on RR1000 Nickel superalloy specimens were modelled using an explicit FE solver in LS-DYNA. The model used in this paper is the same model used to simulate the experimental damage introduced on fatigue specimens in [9]. The FE model geometry and boundary conditions are given in Fig. 1, where symmetry was exploited. The profile of the blunt indenter is generated by two perpendicular surfaces of curvature $R_1 = 12.55$ mm and $R_2 = 1.00$ mm. The springs simulate the compliance of the rig and their stiffness is the only calibrated parameter in the model. The calibration was carried out by choosing the appropriate spring stiffness in order to obtain similar rebound velocity as measured experimentally [9]. The optimal value of the calibrated spring stiffness for the impact velocity range analysed is $k = 3\times10^3$ N/m. The impact velocity was chosen as to obtain dents of 5 and 10 thou depth ($\sim$ 127 and 254 μm) according to the calibration.

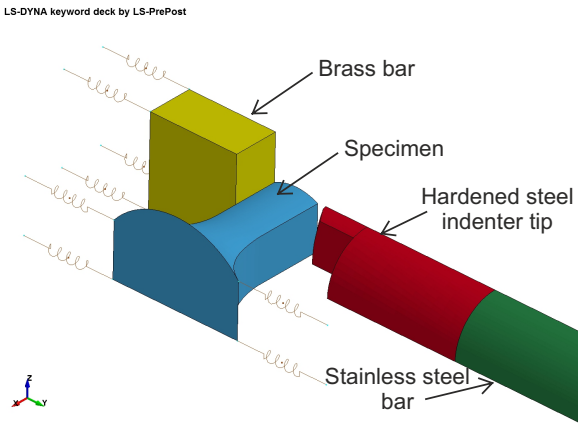

Figure 1: Model geometry and boundary conditions used in the LS-DYNA explicit FE code.

The Nickel superalloy elasto-plastic properties were provided by our industrial collaborator. The room temperature true strain true stress material data was implemented in LS-DYNA as piece-wise linear elastic-plastic Material 24[1]. A purely elastic model was assumed to the hardened steel indenter and an elastic perfectly plastic material model was used to simulate the deformation of the supporting brass bar behind the specimen. The material properties used for the brass block are: $E = 97$ GPa, $\nu = 0.31$ and $\sigma_Y = 150$ MPa. Linear hexagonal elements with reduced integration were used with a final mesh size near the centre of the notch of $h_e = 0.05$ mm. A stiffness based hourglass energy was added to the elements in order to avoid hourglass modes of deformation. The hourglass energy was kept below 10% of the total energy in order to reduce its impact in the final deformation of the dent.

2.2. *Residual stress and dent geometry*

The residual stress field generated under the dent during the impact of the striker was obtained by the FE model in LS-DYNA. The dynamic analysis of the impact of the indenter did not include any damping and, hence, a 'springback' static analysis was carried out at the end of the dynamic step in order to obtain the residual stresses in unloaded equilibrium. A typical field distribution of the the stress component σ_{xx} under the dent is displayed in Fig. 2a. Note that the fatigue load direction is also along the x-direction. A significant compressive zone may be observed under the dent, while the root of the dent is under tensile stress. It is clear from the results in Fig. 2 that whilst the tensile stress under the root will accelerate crack initiation and growth, the compressive zone will slow down the crack propagation. Note that the dent geometry behaves like a notch causing a geometrical stress concentration, which will accelerate the crack growth. The geometrical effect of the notch and the compressive residual stress will have an opposite competing effect on the crack propagation and under certain conditions crack arrest may be observed.

The stress under the centre of the dent along the depth, y, measured from the root of the dent is shown in Fig. 2b for dent depths of 5 and 10 thou. The main difference in stress profile under the

[1]Due to the confidentiality agreement between the University of Oxford and Rolls-Royce plc we are unable to provide the exact elastic-plastic material data of the RR1000 alloy used in this analysis.

dent between the two dent depths is the extent of the compressive zone, although the 5 thou dent residual stress profile also show higher compressive stresses under the dent. These results have been validated by comparison with residual stresses measured by laboratory XRD [9]. The results displayed in Fig. 2b will be used in Section 3.3 in order to calculate the stress intensity factors of a crack propagating in the presence of the residual stress field predicted by the FE model.

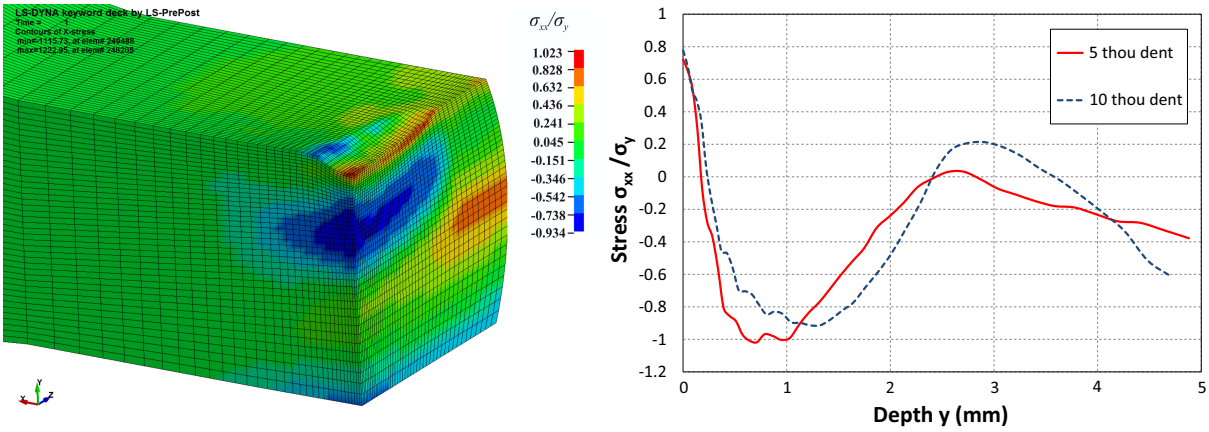

(a) (b)

Figure 2: (a) Contour plot of residual stress σ_{xx} from the FE model; (b) FE results of the σ_{xx} residual stress distribution under the notch root for 5 and 10 thou dents.

The geometry of the dent is also relevant in the calculation of the stress intensity factor of a crack propagating under a notch. Three parameters characterise the 'notch' (i.e. dent) created due to the impact: i) the depth of the notch; ii) the radius of the notch root; and iii) the notch angle (Fig. 3). The notch depth, d, is the deepest point of the dent. The notch angle is 2θ and from the FE results it was found that $\theta \simeq 65^\circ$ for all dent depths. The value of the notch root radius is $\rho = 1.3$ mm, which was measured from the FE results. This is slightly higher than the radius $R_2 = 1.1$ mm of the indenter. An important parameter necessary for the stress intensity factor analysis due to the notch is the ratio ρ/d. These were found to be $\rho/d = 10.2$ for the 5 thou dent and $\rho/d = 5.1$ for the 10 thou one.

3. Stress intensity factor calculation

3.1. Dislocation density method

The input for the crack growth rate model given in Eq. (9) is the stress intensity range at the crack tip. A dislocation density approach is used for the calculation of the stress intensity factor of a crack propagating under a notch (i.e. dent). This approach is for two-dimensional problems. However, although the geometry of the dent is not two-dimensional, at the centre of the notch plane-strain approximation may be used with little loss of accuracy. The approach was first formulated by [15, 16] for two-dimensional cracks and slots. It has also been applied to notches due to FOD [13]. The approach uses dislocations, i.e. displacements discontinuities, to

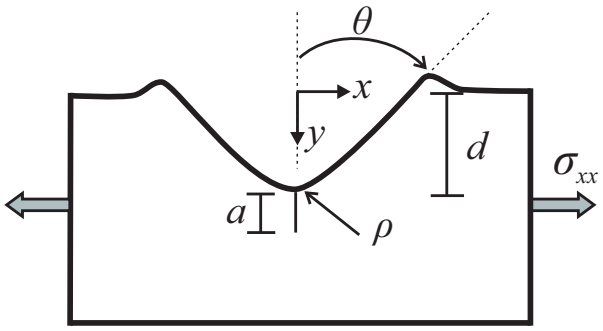

Figure 3: Schematic representation of the geometry of the 'notch' (i.e. dent).

simulate the stress free boundaries of the notch and the crack. The stress components σ_{ij} due to a dislocation at an arbitrary point (x_d, y_d) is given by

$$\sigma^d_{ijk} = \frac{\mu}{\pi(\kappa+1)} b_k G_{kij}(x, x_d, y - y_d), \tag{1}$$

where b_k are the components of the Burgers vector, μ is the shear modulus and κ is the Kosolov's constant (for plane strain $\kappa = 3-4\nu$). G_{kij} are algebraic functions given explicitly in [15]. However, instead of introducing individual dislocations, a continuous distribution of Burgers vector densities, B_x and B_y, are placed along the boundary of the notch and crack in order to obtain the traction free boundaries needed; the stresses due to the dislocations should cancel the original unsatisfied tractions at the edges such that the normal and shear tractions at the boundaries are zero.

For a notch under a crack, the equations that need to be satisfied along the notch boundary, s, and crack length, a, are given by

$$\int_0^s B_x G_{xn}(x, x_d, y, y_d, \phi)dt + \int_0^s B_y G_{yn}(x, x_d, y, y_d, \phi)dt + \int_0^a B_y G_{yn}(x, x_d, y, y_d, \phi)dr + \frac{\pi(\kappa+1)}{\mu}\sigma_n = 0, \tag{2a}$$

$$\int_0^s B_x G_{xs}(x, x_d, y, y_d, \phi)dt + \int_0^s B_y G_{ys}(x, x_d, y, y_d, \phi)dt + \int_0^a B_y G_{ys}(x, x_d, y, y_d, \phi)dr + \frac{\pi(\kappa+1)}{\mu}\sigma_s = 0, \tag{2b}$$

$$\int_0^s B_x G_{xn}(x, x_d, y, y_d)dt + \int_0^s B_y G_{yn}(x, x_d, y, y_d)dt + \int_0^a B_y G_{yn}(x, x_d, y, y_d)dr + \frac{\pi(\kappa+1)}{\mu}\sigma_0 = 0, \tag{2c}$$

where σ_n and σ_s are the normal and shear stresses on the notch boundary and σ_0 is the remote stress applied. Due to the square-root singularity at the crack tip, the problem can be solved by Gauss-Chebyshev quadrature, which is appropriate for singular Cauchy integral equations. Further explanations about the numerical integration used can be found in [13]. The Burgers vector

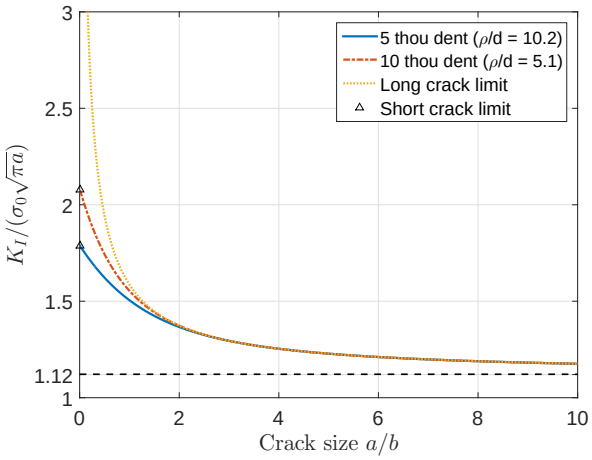

Figure 4: Stress intensity factor due to the notch for a crack propagating under 5 and 10 thou depth dents.

densities are modelled as a bounded function Φ_k and a weight function and can be written as

$$B_k = \Phi_k(t)\sqrt{\frac{1+t}{1-t}}. \tag{3}$$

Once the numerical integration of Eq. (2) is carried out, the stress intensity factor can be obtained as

$$K = 2\sqrt{2\pi a}\frac{\mu}{\pi(\kappa+1)}\Phi_y(1). \tag{4}$$

The residual stresses already satisfy the condition of free tractions on the notch boundary and only the normal stresses due to the crack need to be cancelled. However, by clearing the normal stresses on the crack surface, unsatisfied stresses will be created on the notch boundary, which themselves need to be cancelled [13]. Hence, there are three sets of equations to be solved for a crack propagating under a notch and in the presence of an initial residual stress field.

3.2. Notch stress intensity factor

Using the dislocation density described in Section 3.1, the stress intensity factor of a crack propagating under the 5 and 10 thou dents were obtained. These are displayed in Fig. 4 along with the long crack limit, i.e. the limit of an infinitely sharp crack at the edge of the body. Far from the notch, all three curves converge to the limit of the geometrical multiplier of the stress intensity factor for small surface cracks, $Y = 1.1215$. By using the dislocation density approach, the only input for the stress intensity factor solution in Fig. 4 is the geometry of the 'notch'; namely, the ratio ρ/d and the notch angle θ. Note that the dislocation density approach is indeterminate at the root of the notch, $y = 0$, and the values were obtained from a range of $a/b = 0.01$ to $a/b = 10$.

The stress concentration under the centre of the dent may also be obtained by the dislocation density approach [13]. The stress concentration factor, $K_t = \sigma_{max}/\sigma_0$, at the root of a notch of similar geometry to the dents, same ρ/d, was obtained. The stress concentration factor may be

used to estimate the value of the normalised K_I at the root of the notch, such that,

$$K_I = Y K_t \sigma_0 \sqrt{\pi a}. \tag{5}$$

The stress intensity factor obtained by Eq. (5) provides another bound, a short crack limit, to the K_I values at the root of dents. The values of the stress concentration factors and stress intensity factors at the root of the dent are given in Table 1. The values calculated from the stress concentration factor agree with the normalised K_I results of Fig. 4.

Table 1: Stress concentration and stress intensity factors for the 5 and 10 thou dents.

Dent depth	ρ/d	K_t	$K_I/\sigma_0\sqrt{\pi a}$
5 thou (127μm)	10.2	1.596	1.789
10 thou (254μm)	5.1	1.854	2.079

3.3. Stress intensity factor with residual stress

The presence of a residual stress field will also have a contribution to the stress intensity factor of a crack propagating under the dent. In order to obtain the normalised K_I due to the presence of the residual stress, the residual stress field is assumed to be driving the stress intensity factor of a propagating crack, instead of the remote loading, σ_0. The distribution of the residual stress field obtained with the FE model, shown in Fig. 2b, is used with the dislocation density approach of Section 3.1. However, here, the residual stress, σ^r_{xx}, is normalised by the yield stress of the material at room temperature, σ_Y. Therefore, the normalised stress intensity factor is given by $K_I/\sigma_Y\sqrt{\pi a}$, with σ_Y instead of the remote stress applied, σ_0.

The stress intensity factor evolution of a propagating crack in the the residual stress field is displayed in Fig. 5. The compressive zone near the root of the dent gives rise to a negative stress intensity factor. In the presence of a negative ΔK, the crack is assumed to arrest and no propagation occurs. Therefore, for a crack to propagate, the contribution of the stress intensity factor due to the notch geometry and the applied remote stress needs to be sufficient to overcome the compressive K_I due to the residual stress field. Superimposing the results of Fig. 5 and Fig. 4, it is found that crack arrest will occur for applied stresses lower than $\sigma_0/\sigma_Y = 0.7$ for the 10 thou dent and $\sigma_0/\sigma_Y = 0.8$ for the 5 thou dent. These extremely high loads necessary for a crack propagation are likely to be overestimated due to the absence of residual stress relaxation in this analysis, which is further discussed in Section 4.

4. Fatigue crack growth method

4.1. El Haddad model for short cracks

Surface damage such as dents and scratches have high stress concentration under the damage root, which is known to significantly change the fatigue behaviour of metals [17]. Some of the methods available for evaluating fatigue strength in problems with high stress concentration are

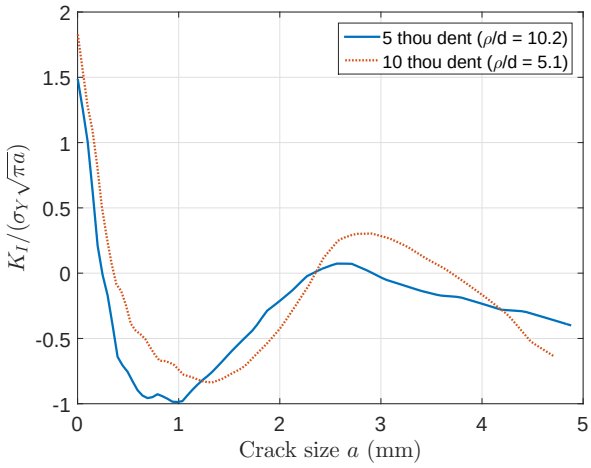

Figure 5: Stress intensity factor due to residual stresses for a crack propagating under 5 and 10 thou depth dents.

the methods based on a critical distance, such as the point, line and area methods [18]. These are often used in conjunction with the El Haddad characteristic length dimension

$$a_0 = \frac{1}{\pi}\left(\frac{\Delta K_0}{\Delta\sigma_f}\right)^2, \tag{6}$$

where ΔK_0 is the stress intensity factor range threshold and σ_f is the fatigue limit. Both these parameters are often considered to be material properties. However, many alloys, including Nickel superalloys, often have no clear fatigue limit and a common practice is to assume the fatigue load at 10^7 as the fatigue limit of the material. The length dimension in Eq. (6) can be seen as a characteristic length dimension of the material.

The short crack method used here derives from the modification of the Kitagawa-Takahashi (K-T) diagram [19] by El Haddad et al. [20] and it has been previously used on dents caused by FOD [5, 14, 21]. A similar modified short crack growth law has been suggested by Pugno et al. [22]. By including a fictitious crack of length, a_0, El Haddad obtained a smoother transition between long and short crack regimes, instead of the sharp transition between the two regimes given by the K-T diagram. The approach suggests that a corrective stress intensity factor represents better the short crack behaviour. This corrective stress intensity range is given by

$$\Delta K_{eff} = Y\Delta\sigma\sqrt{\pi(a + a_0)}, \tag{7}$$

where Y is the geometrical parameter and for surface cracks, $Y = 1.1215$. Note that for large crack lengths, $a \gg a_0$, Eq. (7) will converge to Irwin's stress intensity factor equation near the crack tip.

The simplicity of this approach is that the modified stress intensity range, ΔK_{eff}, given by Eq. (7) can easily be used with Paris law parameters for crack growth. The original Paris law is given by

$$\frac{da}{dN} = C\,(\Delta K)^m, \tag{8}$$

where C and m are material parameters that can be obtained experimentally. Substituting the stress intensity range by Eq. (7), the modified Paris law becomes

$$\frac{da}{dN} = C\left(\Delta K\sqrt{1+\frac{a_0}{a}}\right)^m . \tag{9}$$

However, the crack length ratio may also be written in terms of the applied fatigue load as

$$\frac{a_0}{a} = \left(\frac{\Delta K_0}{\Delta K}\frac{\Delta\sigma}{\sigma_f}\right)^2 , \tag{10}$$

and by substituting Eq. (10) in Eq. (9), one obtains the crack growth rate curve for different applied stress ranges. These results are presented in Fig. 6. It can be observed, as expected, that for $\Delta\sigma/\sigma_f = 0$, the Paris law is recovered. The crack growth rate is higher for short cracks, i.e. $\Delta K < \Delta K_0$, which is the expected behaviour in the presence of high stress concentrations, as observed, for example, under dents and notches.

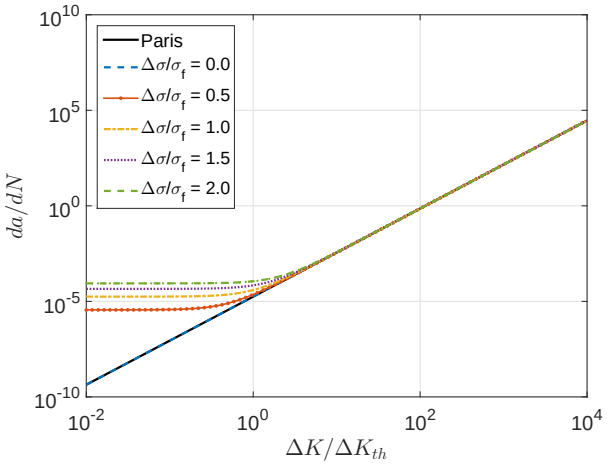

Figure 6: Crack growth law with El Haddad modification for different values of applied load σ/σ_f.

4.2. Fatigue life calculation

In the calculation of the fatigue life in the presence of dents, the stress intensity factors calculated in Section 3.2 are used with the short crack growth model in Section 4.1. A fatigue load ratio of $R = 0$ is assumed in this analysis. However, due to the presence of residual stresses the effective load ratio will vary at each point under the dent, being negative in regions where the stress intensity due to the applied load is insufficient to cancel the negative stress intensity due to compressive residual stresses. The range of stress intensity factor, ΔK, in Eq. (9), is given by the maximum K_I calculated and negative values of K_I are neglected (Fig. 7), since no propagation occur for negative stress intensity factors. The parameters m and C in Eq. (9) are the Paris curve parameters for the RR1000 Nickel superalloy used at room temperature. The fatigue life was then obtained by numerical integration of Eq. (9) for different applied remote loading, σ_0.

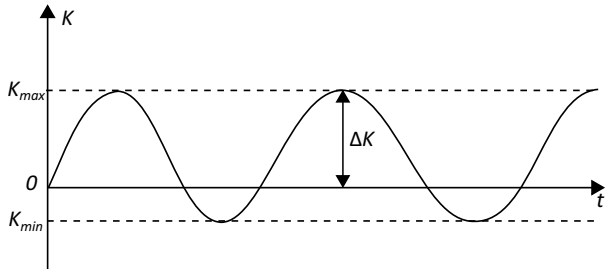

Figure 7: Stress intensity factor range ΔK.

The results for both dent depths are presented in Fig. 8. The curves in the absence of residual stresses are also presented for comparison. By taking into account the residual stresses, the predicted fatigue life increases by a factor of approximately 10 at higher applied loadings. Furthermore, the fatigue limit becomes the load necessary to cancel the effect of the compressive residual stress under the root. As expected, a longer fatigue life is obtained for the 5 thou dent when compared with the 10 thou dent. The higher fatigue limit for the 5 thou dent is due to the higher compressive stresses after the impact shown in Fig. 2b. The values of the fatigue limit for the dented samples in the presence of residual stresses is, however, excessively high. This is due to the lack of residual stress relaxation in the analysis. During the first fatigue load cycle, some of the higher stresses will reach the yield limit and the magnitude of the residual stress distribution is expected to decrease. For high temperature fatigue tests, the change in material properties, such as Young's modulus and yield stress, will also relax some of the high residual stresses observed.

The fatigue life curve predicted with the standard Paris crack growth rate model is also given in Fig. 8. These were obtained without the presence of residual stresses. The comparison between the predicted fatigue life of the modified El Haddad model and Paris show that the short crack model predicts shorter lives. These more conservative results are expected since for low values of ΔK, $\Delta K < \Delta K_0$, the crack growth rate of the modified El Haddad method is higher than that obtained by Paris. The higher crack growth rate is also the reason the difference between the two dent depths is less accentuated with the modified El Haddad method. Hence, the difference between the predicted fatigue life for the 5 and 10 thou dents, taking into account the residual stresses during impact, is mainly due to the contribution of the residual stress field on the stress intensity factor of a propagating crack under the dent.

5. Discussion

The dislocation density approach presented here may easily be implemented in combination with residual stresses obtained via FE analysis to estimate the fatigue life of dented components. However, it will be appreciated that the 2D approach is a simplification of the real 3D situation loading to the 3D damaged model, in the absence of the residual stresses, to evaluate the geometrical stress concentration under the centre of the dent (Fig. 9a). The results may be compared with the stress concentration predicted by the dislocation density method for a notch of similar angle θ and ratio ρ/b. In the dislocation density method, the stresses due to the presence of the notch (only) may be obtained by removing the components due to the stress free boundary of the crack

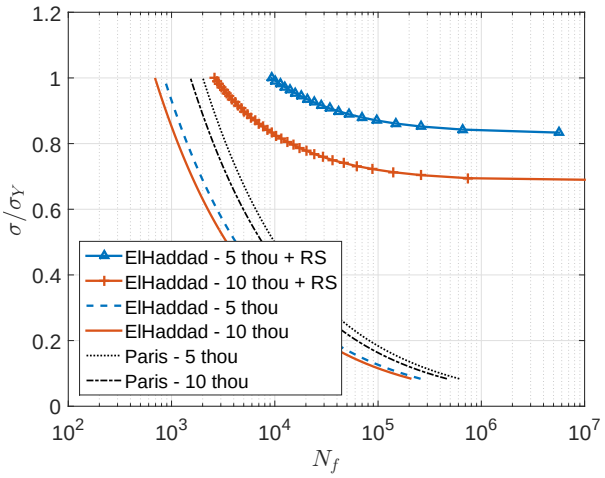

Figure 8: Predicted fatigue life for the 5 and 10 thou dents with and without residual stresses.

in Eq. (2) [13]. The results of the stress component σ_{xx} under the dent obtained both with the dented 3D FE model in ABAQUS, without residual stresses, and with the 2D dislocation density approach are presented in Fig. 9b. The σ_{xx} distributions obtained are very similar in form and at no point is the relative error between the two solutions greater than 5%. These results therefore validate the assumption used that, at least at its centre, the dent may be approximated by a 2D 'V' notch in plane strain.

The second question, regarding the accuracy of the line crack propagating under the dent, is much more difficult to assess. In reality, the propagation of the crack is three-dimensional and, although the dislocation density method has similar counterparts for 3D problems, the implementation and solution of these methods are complex and fall outside the scope of this paper. Other techniques such as extended finite element would present a more viable approach. However, the assumption made here is that, although the residual stress field makes the problem multi-axial, the crack will propagate primarily under mode I loading, since the specimens in question will be submitted to uni-axial loading. The crack will therefore propagate in the plane perpendicular to the loading and, because of the geometry of the dent, the crack will grow very quickly along the bottom of the dent. Hence, a high aspect ratio crack will form early on in the fatigue life, and modelling further propagation in a 2D plane strain framework would seem reasonable. The effect of the a 3D crack in more complex loadings, as well as direct comparison with experimental data are topics that we intend to investigate in future work.

6. Conclusions

The effect of blunt dents on the fatigue life were investigated here. Blunt dents may be introduced to components during manufacturing and maintenance, and the effect on fatigue life of the geometrical stress concentrator introduced and the residual stress created during the impact were studied. The FE model validated in [9] was used in this paper to obtain the dent geometry and stress field generated after low velocity impacts of hard blunt objects. A dislocation density approach was then used to calculate the stress intensity factor of a crack propagating under dents

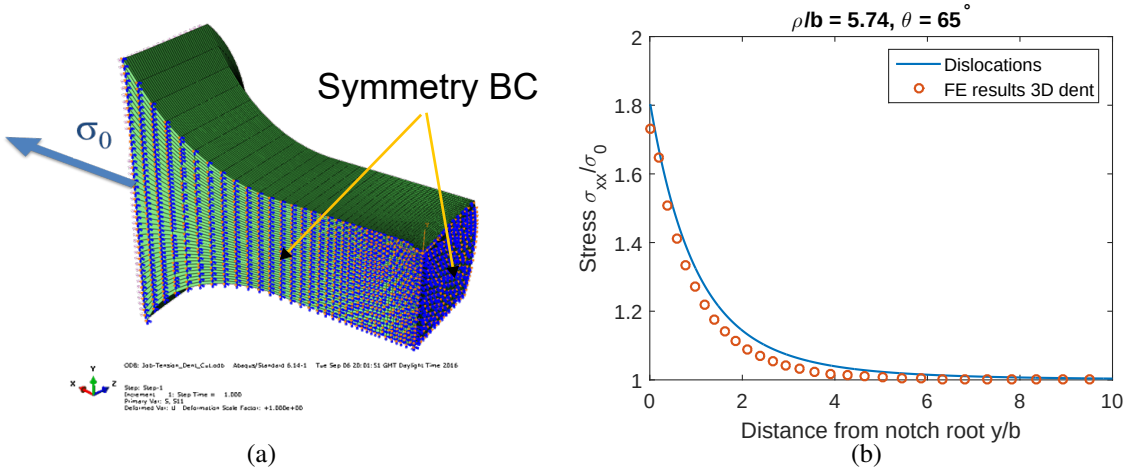

(a) (b)

Figure 9: (a) Three-dimensional FE model of damaged specimen without residual stress; (b) Comparison of σ_{xx} stress results under the notch root due to the stress concentrator only between 3D FE model result, at the centre of the dent, and the 2D dislocation approach.

of 5 and 10 thou depths. Both the contributions of the geometrical stress concentrator and the residual stress field to the stress intensity factor of a crack under the dent were obtained. Superposition was then used to obtain the effective stress intensity range for the crack growth calculations. The dislocation density approach used is a two-dimensional approach and the 'notch' created by the dent is assumed to be in plane-strain. Although the dent mark created after impact is a three dimensional geometry, at the centre of the dent plane-strain assumption can be used with little loss of accuracy.

The fatigue life was then calculated using Paris law for crack growth rate and a modified El Haddad model for short cracks. The short crack model used in this paper assumes a constant, but higher than Paris, crack propagation rate for low values of ΔK and, hence, shorter fatigue lives are predicted with this model. It was also shown that the residual stresses are responsible for a significant increase in the predicted fatigue lives. Both depths of dent have shown higher fatigue lives in the presence of residual stresses, despite the high tensile stress at the root of the dents. High fatigue limits were also observed for both dents, which represent the necessary remote load for the contribution of the stress intensity factor due to the notch geometry to cancel the negative stress intensity due to the compressive residual stress under the dent. The need to take into account residual stress relaxation mechanisms, such as due to the first fatigue cycle and temperature increase, is therefore essential for an appropriate comparison between the predicted fatigue lives with experimental results.

7. Acknowledgements

The authors would like to thank Innovate UK and Rolls-Royce plc for the financial support to this work.

References

[1] S. Mall, J. L. Hamrick, and T. Nicholas. High cycle fatigue behavior of ti–6al–4v with simulated foreign object damage. *Mechanics of materials*, 33(11):679–692, 2001.

[2] S. Gourdin, J. Cormier, G. Henaff, Y. Nadot, F. Hamon, and S. Pierret. Assessment of specific contribution of residual stress generated near surface anomalies in the high temperature fatigue life of a rené 65 superalloy. *Fatigue & Fracture of Engineering Materials & Structures*, 2016.

[3] L. Doremus, J. Cormier, P. Villechaise, G. Henaff, Y. Nadot, and S. Pierret. Influence of residual stresses on the fatigue crack growth from surface anomalies in a nickel-based superalloy. *Materials Science and Engineering: A*, 644:234–246, 2015.

[4] B.L. Boyce, X. Chen, J.W. Hutchinson, and R.O. Ritchie. The residual stress state due to a spherical hard-body impact. *Mechanics of Materials*, 33(8):441–454, 2001.

[5] D. Nowell, P. Duo, and I.F. Stewart. Prediction of fatigue performance in gas turbine blades after foreign object damage. *International journal of fatigue*, 25(9):963–969, 2003.

[6] P. Duo, J. Liu, D. Dini, M. Golshan, and A.M. Korsunsky. Evaluation and analysis of residual stresses due to foreign object damage. *Mechanics of materials*, 39(3):199–211, 2007.

[7] P.G. Frankel, P.J. Withers, M. Preuss, H.T. Wang, J. Tong, and D. Rugg. Residual stress fields after fod impact on flat and aerofoil-shaped leading edges. *Mechanics of Materials*, 55:130–145, 2012.

[8] S. Zabeen, M. Preuss, and P.J. Withers. Residual stresses caused by head-on and 45 foreign object damage for a laser shock peened ti–6al–4v alloy aerofoil. *Materials Science and Engineering: A*, 560:518–527, 2013.

[9] R.M.N. Fleury, D. Nowell, T. Sui, S. Ying, A.M. Korsunsky, Y.H. Tai, and F. Silva. Characterisation of handling and service surface damage on nickel alloys caused by low velocity impacts of blunt hard objects. *Mechanics of Materials*, 107:45–55, 2017.

[10] J. Ding, R.F. Hall, J. Byrne, and J. Tong. Fatigue crack growth from foreign object damage under combined low and high cycle loading. part i: Experimental studies. *International journal of fatigue*, 29(7):1339–1349, 2007.

[11] J. Ding, R.F. Hall, J. Byrne, and J. Tong. Fatigue crack growth from foreign object damage under combined low and high cycle loading. part ii: A two-parameter predictive approach. *International journal of fatigue*, 29(7):1350–1358, 2007.

[12] J.O. Peters, B.L. Boyce, X. Chen, J.M. McNaney, J.W. Hutchinson, and R.O. Ritchie. On the application of the kitagawa–takahashi diagram to foreign-object damage and high-cycle fatigue. *Engineering fracture mechanics*, 69(13):1425–1446, 2002.

[13] D. Nowell, D. Dini, and P. Duó. Stress analysis of v-notches with and without cracks, with application to foreign object damage. *The Journal of Strain Analysis for Engineering Design*, 38(5):429–441, 2003.

[14] S.Y. Oakley and D. Nowell. Prediction of the combined high-and low-cycle fatigue performance of gas turbine blades after foreign object damage. *International journal of fatigue*, 29(1):69–80, 2007.

[15] D. Nowell and D.A. Hills. Open cracks at or near free edges. *The Journal of Strain Analysis for Engineering Design*, 22(3):177–185, 1987.

[16] D. Nowell. Strain changes caused by finite width slots, with particular reference to residual stress measurement. *The Journal of Strain Analysis for Engineering Design*, 34(4):285–294, 1999.

[17] S. Suresh. *Fatigue of materials*. Cambridge university press, 1998.

[18] D. Taylor. Geometrical effects in fatigue: a unifying theoretical model. *International Journal of Fatigue*, 21(5):413–420, 1999.

[19] H. Kitagawa and S. Takahashi. Applicability of fracture mechanics to very small cracks or the cracks in the early stage. In *Second International Conference on Mechanical Behavior of Materials. ASM, Metals Park, Ohio. 1976, 627-631*, 1976.

[20] M.H. El Haddad, T.H. Topper, and K.N. Smith. Prediction of non propagating cracks. *Engineering Fracture Mechanics*, 11(3):573–584, 1979.

[21] P. Duo, D. Nowell, and J. Schofield. Assessment of foreign object damage (fod) to aero engine blades. In *Proceeding of the 9th National Turbine Engine HCF Conference, Pinehurst, NC*. Citeseer, 2004.

[22] N. Pugno, M. Ciavarella, P. Cornetti, and A. Carpinteri. A generalized paris law for fatigue crack growth. *Journal of the Mechanics and Physics of Solids*, 54(7):1333–1349, 2006.